An Experimental Study of Evaporative Cooling from Liquid Droplets Impinging on a Hot Surface

by

Catherine Helene Koveal

Submitted to the Department of Mechanical Engineering in Partial Fulfillment of the Requirements for the Degree of

Bachelor of Science

at the

Massachusetts Institute of Technology

June 2005

Signature of Author .....
Department of Mechanical Engineering
May 6, 2005

Certified by .....
Anette Hosoi
Assistant Professor of Mechanical Engineering
Thesis Supervisor

Accepted by .....
Ernest G. Cravalho
Chairman, Undergraduate Thesis Committee

An Experimental Study of Evaporative
Cooling from Liquid Droplets Impinging on a Hot Surface

by

Catherine Helene Koveal

Submitted to the Department of Mechanical Engineering
on May 6, 2005 in Partial Fulfillment of the
Requirements for the Degree of Bachelor of Science in
Mechanical Engineering

ABSTRACT

We have performed a series of experiments to characterize the different regimes observed in drop impacts during evaporative cooling of heated surfaces. We found four regimes which were named splashing, fizzing, flat film, and marbling based on the dynamic properties of the drop impact. We found that the emergence of these regimes is primarily controlled by the Jacob number, a dimensionless group describing the ratio of sensible to latent energy absorbed during liquid-vapor phase change. Using our classification scheme, we can predict a range of useful Jacob numbers to use in the cooling of electronic components. From these Jacob numbers, we can extract the material properties of a fluid required to cool a given system.

Thesis Supervisor: Anette Hosoi
Title: Assistant Professor of Mechanical Engineering

Table of Contents

Nomenclature

σ	surface tension, N/m	***We***	Weber Number, $\rho v^2 D/\sigma$
ρ	density, kg/m^3	***Re***	Reynold's Number, $\rho vD/\mu$
μ	viscosity, kg/ms	***Ja***	Jacob Number, $(T_s-T_b)cp/L$
L	heat of vaporization, kJ/kg	***f***	frequency, drops/s
k	thermal conductivity, W/mK	***D***	diameter, m
α	coefficient of thermal expansion, 10^{-6}/˚C	***v***	velocity, m/s
Tb	boiling point, ˚C	***Cpf***	fluid specific heat, J/kgK
Ts	substrate temperature, ˚C	***Cps***	substrate specific heat, J/kgK

1.0 Introduction

Evaporative cooling has become a thermodynamic research focus in recent years because of its potential to dissipate high heat fluxes (as much as 40 kW/m^2) at an affordable cost. Technological advances in areas such as electronics, lasers, and metallurgy are creating challenges of non-uniform heat fluxes and high surface temperatures that traditional cooling methods cannot handle. Especially in computer electronics, processor segmentation into hot spots surrounded by much cooler caches creates a need for high heat dissipation in specific locations unachievable by airflow through a heat-sink. Without adequate cooling, the devices will have reliability problems or even failure due to overheating.

Compared to single-phased forced convection, the liquid-vapor phase change during evaporative cooling creates a much higher heat transfer from the hot substrate to the cooler fluid. In the two-phase cooling process, droplets of liquid impact the heated surface and undergo phase change through one of the boiling regimes. The heat of vaporization of the working fluid determines the amount of heat that can be removed from the hot substrate during the evaporation process. The degree of surface cooling also depends on the area coverage of the droplet as well as the heat flux through the substrate. The goal of this form of cooling in industrial applications is to

maintain an approximately uniform temperature safely below a defined critical value by wetting the surface with a mist of droplets.

Although this would be a new application for droplet sprays, the phenomenons of spray generation and drop-surface impact have been studied for years. Sprays have been used in aerosols, airbrushes, and inkjet printing, just to name a few applications. However, on a more fundamental level, the sprays are just droplets of a uniform size and speed delivered by a carrier gas. Upon impact with a hot surface, the drops may remain cohesive, shatter into smaller parts, or spread out on the surface before evaporating. This surface interaction is determined by the impact energy, fluid and substrate properties, and the temperature of the surface. At a liquid-dependent point called the Leidenfrost Temperature, the droplet undergoes maximum evaporation time due to the vapor cushion separating the liquid from direct wall contact. Below the Leidenfrost point, the liquids undergo nucleate and transition boiling, while above this point, film boiling occurs.

2.0 Previous Work

2.1 Drop Visualization

Chandra and Avedisian [1] used high-speed flash photography to study the influence of surface temperature on the shape of n-heptane droplet impacts. The photos allowed them to visualize drop flattening and spreading and as well as vapor bubble formation for drops with We = 43 impacting a polished stainless steel surface. They concluded that the impact shapes were highly temperature dependent over the experimental range of 24-250°C.

Makino and Michiyoshi [2] used high-speed photography to measure the contact and waiting (time between impact and boiling) periods of low-velocity water droplets impacting a hot substrate surface. For water droplets at 0.3 m/s with diameters ranging between 2.54-4.50 mm and

surface temperatures from 150-360°C, the paper concluded that, on impact, the drop spreads out into a thin film before boiling off. They used the sequential images and the frame rate to assess the duration of drop-surface contact and time interval between impact and boiling initiation.

Inada, Miysaka, Sakamoto, and Hojo [3] used laser optics to measure the thickness of the vapor film formed from impacts of water drops, We = 12-15, on a 180-500°C copper surface. They measured film thicknesses of 5 μm for water at 88K and 10 μm for water at 2K.

Bernardin, Stebbins, and Mudawar [4] used photographic images to show that nucleate boiling occurs prominently occurs at the rim of the disk of impacted fluid even though it may not be able to be sustained by the majority of the surface area. This results in a non-uniform heat transfer over the wetted area. This paper also observed the onset of boiling before the drop reached maximum impact diameter, implying that the heat flux during the spreading stage could be significant.

Hsieh, Fan, and Tsai [5,6] used water and R-134a droplets of diameters 22.7-79 μm impacting a copper substrate at 60-250°C to develop transient cooling and nucleate boiling curves. They concluded that mass flux strongly influences cooling performance and that water allows for greater heat transfer than R-134a.

2.2 Drop-Surface Thermal Interaction

Karl and Frohn [7] studied the momentum loss, drop deformation, and drop disintegration of water and ethanol impacting a copper substrate in the film boiling regime (around 600K). They determined a momentum loss of 60% normal to the substrate and a minimum impact angle below which the drop remains intact.

Jia and Qiu [8] used fringe probing, produced by the interference of two laser beams, to quantitatively measure the contact diameter of ethanol, water, and surfactant droplets with 7.5 m/s

velocity and diameters ranging from 0.19-0.46 mm. Based on the experimental data, they concluded that the evaporation process can be divided into three stages: 'constant volume heating up, constant diameter evaporation, and constant contact angle evaporation.' They extended their work a year later by identifying three heat transfer regions below the critical heat flux: I. convective cooling, II. thin film boiling, and III. drop-wise impact cooling.

Directed by analysis of thermal equations and experimental observations, Baumeister, Hamil, and Schoessow [9] developed a dimensionless relationship for the vaporization times of liquid droplets in the film boiling regime. This study formed a base for relating heat transfer from droplet spray to impact velocity and drop frequency.

Wachters and Westerling [10] investigated the droplet dynamics and resulting heat transfer of water drops impacting a 400°C horizontal surface in the film boiling regime. The impact velocity remained below the critical value of 5 ft/s for 0.07 in diameter water droplets, so drop breakup on impact was not a factor. The paper asserted that the observations could be grouped into three categories based on *We* number: radial spread and single rebound in low $We \leq 30$ regime; dual drop rebound in $30 < We < 80$ regime; and violent vaporization in $We \geq 80$ regime.

Pedersen [11] used sinusoidal vibrations to produce tiny water droplets on the scale of 200-400 μm impacting the 350-1150°F stainless steel surface at 8-33 ft/s. His research found that, during film boiling, heat flux varies proportionally with droplet velocity and is only minimally affected by changes in substrate temperature since the drop does not wet the surface in this regime.

McGinnis and Holman [12] determined heat transfer rates for individual droplets (larger than 0.01 in diameter) of acetone, alcohol, and water. The paper showed the dependence of the heat transfer rate on the physical properties of the fluids, the component of the impact velocity normal to the substrate surface, and the vapor layer thickness.

Xiong and Yuen [13] used strobe-visualization to study the vaporization of liquid (water, hydrocarbon fuels) droplets with a 0.07-1.8 mm diameter and a 0.4 m/s impact velocity on a stainless steel plate. Additionally, they defined the maximum heat transfer rate at 50-60°C above boiling point.

2.3 Leidenfrost Temperature

The Leidenfrost Temperature is the point immediately before initiation of the film boiling regime where impacting fluid becomes separated from the solid surface by a cushion of vapor. At this point, maximum evaporation time of the fluid occurs.

Baumeister and Simon [14] developed a correlation equation relating liquid properties and initial temperatures to the Leidenfrost point. On stainless steel, the Leidenfrost point for water was 285°C and for ethanol 190°C; on aluminum, water was 230°C and ethanol was 155°C. They determined that the contact angle and degree of surface fouling had the greatest effect on the point, and that liquid subcooling had little effect.

Gottfried, Lee, and Bell [15] proposed an analytical model for the Leidenfrost point based on the theory that heat is transferred to the droplet by conduction through the bottom and radiation to its entire volume and mass is lowered by evaporation on the bottom and diffusion from the top. The Leidenfrost point was found to be independent of drop size and in the range of 100-105°C above the saturation temperature for most pure liquids aside from water.

2.4 Spray Cooling

Ciofalo, Di Piazza, and Brucato [16] used cone-shaped spray nozzles to model the heat transfer as a function of surface and liquid temperature of hot sprays (water) ranging from 13-28 m/s in velocity and from 0.4-2.2 mm in drop diameter. The paper concluded that the heat transfer

coefficient and maximum heat flux depend on mass flux and drop velocity far more than drop diameter.

Kim, You, and Choi [17] applied a microporous surface coating of ABM (aluminum particles/Devcon brushable ceramic epoxy/methyl-ethyl-ketone) to a copper substrate and compared its heat transfer to a polished, flat surface. They found that, for a spray of water droplets from 1.25-2.40 mL/min, the heat transfer coefficient was improved by 400% over uncoated surfaces cooled by air due to the connected microporous cavities in the coating.

3.0 Experimental Setup

3.1 Overall Setup

The setup of the experimental apparatus is shown in Figure 1. The two ring stands with attached clamps support a 1.2 cm thick block of aluminum. The aluminum acts as a platform that can be raised and lowered to create different drop impact velocities due to gravity. The syringe heights tested in this experiment were 9.4, 22.6, 32.6, and 42.6 cm. The 9.4 cm drop was created by placing the syringe pump on top of the aluminum block at ground level. The other three heights were created by positioning the clamps at 10, 20, and 30 cm respectively above the ring stand base.

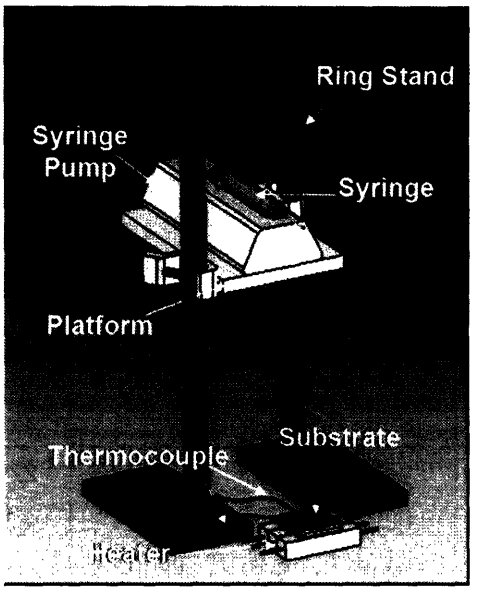

Figure 1: Total experimental setup for evaporative testing.

The pump with fluid-filled syringe was positioned on top of the aluminum plate with the tip of the needle located vertically above the center of the copper substrate. The vertical placement was verified by marking the center of the substrate (intersection of diagonals from the corners) and then repositioning the plate or pump until the drops hit that mark.

The copper substrate and matching base were set directly on top of the resistance heater. The base plate allowed for even heating of the polished substrate surface while protecting the thermocouples reading the heater temperature. The resistance heater was hooked by positive and negative leads to the power source. The voltage was manually varied to produce the range of surface temperatures. The thermocouple leads were attached to the temperature reader so that the output in degrees Fahrenheit could be read directly from the display.

3.1.1 Fluids

This experiment was designed to develop a dimensionless thermal and dynamic correlations for a range of fluids. In this case, acetone (99% min. by GC), ethanol (reagent grade, 95%), and water were chosen because they have boiling points approximately 20°C apart so that

their nucleate and part of their transition boiling phases can be studied individually. Additionally, their varied physical properties allow for testing over a wider range of substrate temperatures and drop sizes. The properties of these fluids used throughout this paper can be found in Table 1. The variables representing the properties are defined in Nomenclature.

Table 1: Physical Properties of Acetone, Ethanol, and Water at 20°C

Fluid	Tb	σ	ρ	μ	L	cp	k
Units	°C	N/m	kg/m3	kg/ms	kJ/kg	J/kg K	W/m K
Water	100.0	0.0728	998	1.00E-03	2258	4200	0.607
Ethanol	78.29	0.0223	789	1.20E-03	838	2400	0.169
Acetone	56.05	0.0238	789.9	3.89E-04	518	2130	0.161

3.1.2 Syringes and Drop Size Calibration

The drop sizes of liquid used in the experiment were varied using three different needle-tip attachments (16 gauge, 20 gauge, 25 gauge) on a 10mL plastic syringe. Although the inner diameters of the needles were known, the drops were allowed to fall from the tip solely under the action of gravity, so the size of the produced drop was a function of the surface tension of the given liquid. To calibrate the tips for each liquid, the number of drops created by a 1mL volume of fluid was counted. The drops were assumed spherical for simplicity, so a drop diameter could be estimated from the volume per drop attained by the calibration. The relationships between fluid, syringe, and drop diameter are found in Table 2.

Table 2: Syringe calibration

Fluid	Syringe	Drops/mL	Drop Diameter
Units	*gauge*		mm
Water	25	39	3.66
	20	25	4.24
	16	15	5.03
Ethanol	25	58	3.21
	20	42	3.57
	16	30	3.99
Acetone	25	56	3.24
	20	38.5	3.67
	16	27.5	4.11

A steady frequency of drop impingement on the substrate was created and controlled by a Harvard Apparatus (Pump 11) single-syringe pump. The filled plastic syringe with tip was loaded into the pump apparatus by hand. The flow rate (mL/min) could be set electronically by user-input and varied throughout the course of the experiment. When activated, the pump would create a pulse-free force on the plunger of the syringe, forcing the liquid out the tip at the preset rate. The rate, and therefore drop frequency, was raised and lowered based on overlap of drops or time lag following evaporation on the substrate surface.

3.1.3 Heater and Power Source

The heat source for substrate temperature variation was created by soldering three ceramic power resistors (Radioshack 20W/8Ω) in series. The bars placed next to each other produced a flat, rectangular surface large enough to fit the dimensions of the copper base plate. The bottom and sides of the resistors were wrapped in adhesive-backed ceramic fiber tape. This tape prevented the heater from scorching the table or accidentally burning anyone if the heater location needed to be adjusted.

The open resistor leads were attached to the power source (HP 3616A 0-35V, 0-1.7A) by retractable-hook cables. The voltage on the power source was set to produce the surface temperature on the substrate. The voltage-to-temperature relation was determined by setting the power source to a given voltage and then allowing the plate temperature to settle to steady state. At steady state, the plate temperature remains constant over time. The calibration plot can be seen in Figure 2.

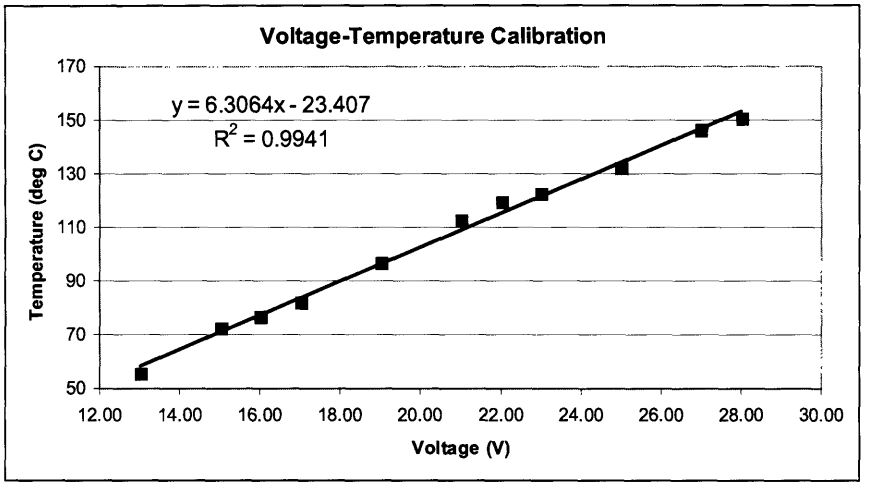

Figure 2: Plot of linear relationship between voltage and surface temperature.

3.1.4 Substrate

In choosing a substrate to act as the surface for drop vaporization, stainless steel, aluminum, glass, and copper were all considered. Glass was ruled out because, although its surface would maintain a smooth finish, it is a poor conductor. Stainless steel was unattractive because it is much harder to machine than either copper or aluminum. Between the final two options, copper was chosen as the substrate because it has a higher thermal conductivity (410 W/mK) than aluminum (237 W/mK) and therefore will better maintain a uniform temperature across its surface and throughout its thickness. The properties of copper (alloy 101) used in this paper can be found in Table 3.

Table 3: Physical Properties of Copper (Alloy 101)

Type	Tm	α	cp	k	ρ
Units	°C	10^-6/°C	J/kg K	W/m K	kg/m3
Copper	1083.4	16.6-17.6	390	410	2600

Additionally, copper is easily polished and milled as required by this application. To maintain a uniform layer for the drop impingement, the top side of the copper plate was polished to

a mirror-finish. However, the finish was not perfect because the copper had some superficial blemishes resulting from rough treatment during shipping of the unfinished metal block.

In order to measure the surface temperature during drop interaction, thermocouples were affixed near the upper surface of the 5cm square copper plate of 3.175 mm thickness. To test for uniform surface temperature during heating and to get an accurate temperature change reading if the drop impacted off-center, four thermocouples were placed in a cardinal pattern around a fifth thermocouple at the center of the copper plate. The milled channels for thermocouple placement are shown in Figure 3.

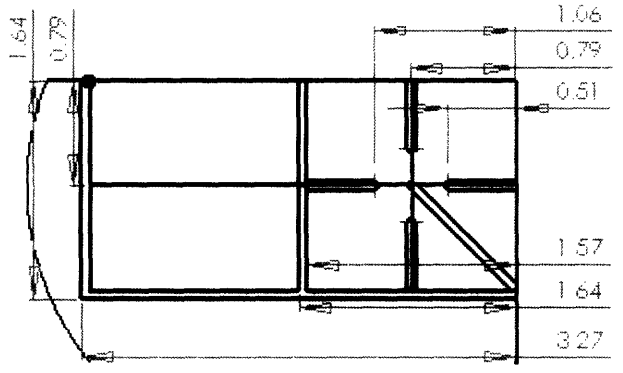

Figure 3: Dimensions and locations of milled thermocouple channels.

The depth and width dimensions of the milled channels were designed to fit the thermocouple wire which had a diameter of 0.81 mm (0.032 in) and the smallest bit available for milling was 0.125 in. The thermocouples used in this application were T-type (Omega 5TC-GG-T-20-36) for compatibility with the temperature measurement device (Omega model 199). The plate setup shown in Figure 4 used two copper plates: a blank copper plate as a flat surface on top of the resistance heaters and another plate of the same dimensions with the milled thermocouple channels.

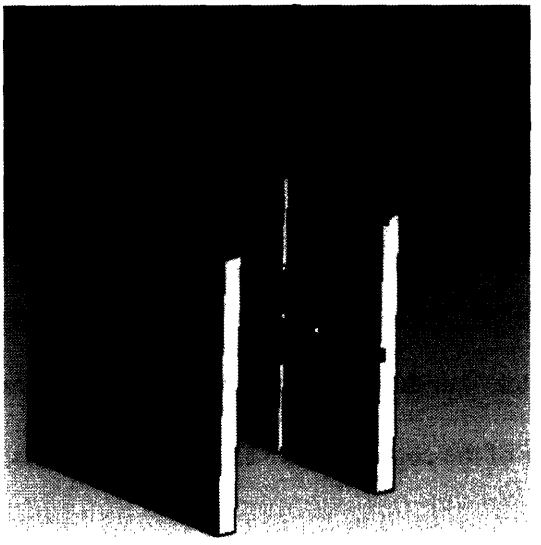

Figure 4: Sandwiching of thermocouples between uniform copper surfaces.

The thermocouples were adhered into the channels with Loctite super glue. The contact between the copper plate and thermocouple tip was verified through a simple multimeter resistance check. An average thermocouple has a resistance of 1.4Ω, so the thermocouple is maintaining good contact if the multimeter reads within 0.5Ω of that value as measured across the Constantan (negative) lead and the copper surface (positive).

3.2 Procedure

Once the apparatus has been arranged as indicated in Figure 1, the experimental process is ready to be initiated in as follows:

1. Polish the copper surface with copper cleaning cream prior to the initial run and after changing fluids to remove the oxidation.
2. Arrange substrate and base plate on top of resistance heater and set power source to required voltage to begin process of heating to steady state.
3. Fill each syringe to maximum capacity with fluid and attach needle tip.
4. Load syringe of fluid being tested into syringe pump and enter flow rate.

5. Set platform to required height and arrange syringe pump such that needle tip is vertically over the center of the substrate.
6. When plate reaches specified temperature, activate pump for 10 drops of fluid.
7. Record fluid, needle tip, height, flow rate, initial surface temperature, temperature change, and drop-surface interaction.

This process was repeated at each of four syringe heights (9.5, 22.6, 32.6, and 42.6 cm above ground level) using each of three needle tips (25G, 20G, 16G) for each of three fluids (acetone, ethanol, and water).

4.0 Theoretical Analysis

4.1 Boiling Regimes

In the course of experimental testing, the substrate temperature was regulated to stay below the Leidenfrost Point. As shown in Figure 5, the Leidenfrost Temperature is the point of minimum heat flux above which the fluid transitions into the film boiling regime. By keeping the surface temperature within the range of 140-260°F, the liquid drops underwent only nucleate or transition boiling so that the drops directly contacted the hot surface.

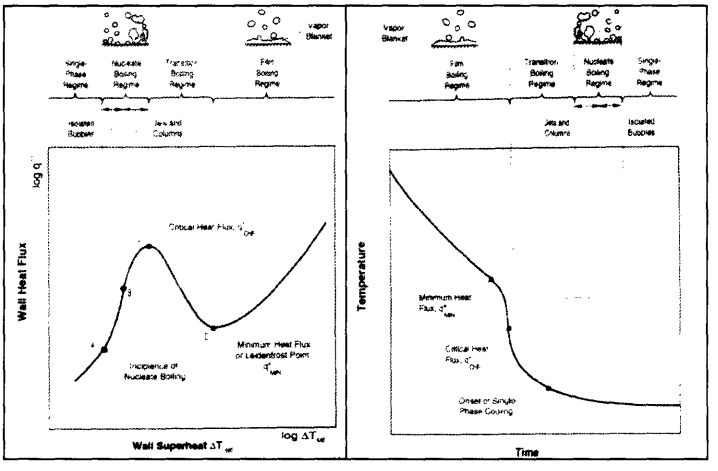

Figure 5: Boiling curve for standing body of liquid [10].

4.2 Buckingham Pi Theorem

To analyze the experimental data, the Buckingham Pi Theorem was used to determine the relationship between important parameters of the system. To begin with, the main goal of evaporative cooling was defined as producing a temperature change. This temperature change was affected by properties of the liquid droplet and the substrate.

For the fluid droplet, the significant parameters were physical properties of the liquid as well as attributes of the droplet. Physically, the surface tension and density mattered because it affected the diameter of the droplet produced by the syringe. The viscosity mattered because it affected the thickness of the liquid layer spread on the substrate surface. The specific heat and latent heat of vaporization of the fluid determined the thermal effect of spraying the substrate with the droplets. The boiling point of the fluid determined the temperature above which evaporative cooling could take place. Also, the velocity affected the drop shattering and the frequency affected the rate of heat removal.

For the substrate, the important parameters were primarily thermal. The initial surface temperature determined the type of boiling the drop underwent upon impact. The specific heat of the surface affected the heat transfer to the liquid drop.

All of these parameters are listed by Equation 1. Any quantity of interest (e.g. temperature change of the surface) will be a function of drop diameter, excess temperature, surface tension, velocity, viscosity, density, specific heat, surface temperature, drop frequency, and latent heat.

$$D, \Delta T, \sigma, v, \mu, \rho, Cp, T_s, f, L \tag{1}$$

As shown in Equation 1, the problem has n=10 variables. By looking at the units of these variables, the problem has m=4 reference dimensions (length L, mass M, time T, and temperature Θ). Thus, there are k=n-m=6 dimensionless π groups that can arise in solutions to this problem.

The first π group, shown in Equation 2, relates the excess temperature of the surface to the latent and specific heat of the fluid. The group implies that the ability of the fluid to conduct and evaporate away heat is coupled to temperature change on the surface. This group is also known as the Jacob number. The Jacob number relates the conductive heat transfer, to the fluid, to the heat removal by evaporation through the difference in surface temperature and liquid boiling point.

$$\Pi_1 = \frac{\Delta T C p}{L} = Ja = \frac{(T_s - T_b) C p_f}{L} \tag{2}$$

The second π group in Equation 3 relates the drop velocity to the drop diameter and impact frequency. The velocity affects the shattering of the single droplet into smaller shards. The diameter multiplied by frequency determines the volume of water impacting the surface and the area for heat transfer.

$$\Pi_2 = \frac{v}{Df} \tag{3}$$

The third π group in Equation 4 relates the temperature change in the system to the initial substrate temperature. This group implies that the difference between initial surface temperature and final temperature after the drop impact may change depending on how hot the surface is to begin with.

$$\Pi_3 = \frac{\Delta T}{T_s} \tag{4}$$

The fourth π group in Equation 5 relates the drop velocity to the fluid's latent heat of vaporization. This correlation connects the drop's kinetic energy to its evaporation energy.

$$\Pi_4 = \frac{v^2}{L} \tag{5}$$

The fifth π group, also known as the Weber number, relates the drop's inertia to its surface tension. Basically, the group implies that higher surface tension will require a greater impact to break it apart.

$$\Pi_5 = \frac{\rho v^2 D}{\sigma} = We \tag{6}$$

Finally, the sixth π group, also known as the Reynold's number, relates the drop's inertia to its viscosity.

$$\Pi_6 = \frac{\rho v D}{\mu} = \mathrm{Re} \tag{7}$$

Although the above π groups can be formed from what were considered the important parameters, not all groups ended up having an impact in this experiment. Part of the experimental process was to determine which parameters were related and informative.

5.0 Experimental Results

5.1 Drop Impact Progression

A Phantom v4.2 High-Speed Digital Camera by Visible Solutions was used to generate 512x512 pixel images of the liquid drops impacting the substrate surface. A high-speed camera was required because the spherical drops rapidly flatten into disks on impact and evaporate quickly if the substrate temperature is above the fluid boiling point. With this camera, the drop impacts were recorded as a video at 200 pps (pictures per second) with the camera angled at the substrate surface. The software allows a user to step through the video frame by frame and save the images as short films or individual jpegs. For this experiment, images from the first 10-15 frames after surface contact were saved and chronologically organized to study impact phenomenon as a function of surface temperature and height.

Impacts were recorded for droplets of each of the three fluids (acetone, ethanol, and water) falling from the highest (42.6 cm) and lowest (9.5 cm) heights while the substrate temperature was varied at 10 degree intervals above boiling point. The complete photo record of drop impacts can be found in the Sections 8.4-8.6.

The impacts of ethanol droplets from a 20 gauge syringe at 42.6 cm high will be used as an example of the trends seen across all fluids tested. For ethanol, the boiling point is 173°F (78.3°C), so pictures were taken for 10°F steps from 180-210°F.

Figure 6 shows the evolution of an ethanol droplet released from 42.6 cm high onto an 180°F copper surface. The droplet flattens into a disk immediately after touching the surface and the fluid contracts into a ring with globules in the center. The light reflected off the fluid shows that the drop remains as a puddle while it gradually boils off.

Figure 6: Ethanol droplet impacts at 180°F.

Figure 7 shows a similar volume droplet impacting at 190°F. The drop initially flattens in the same way as at 180°F, but the rim flattens as it pulls into a flower shape of separate pools. The glare off the peaks shows that the drop still has a significant volume of water, but the haziness implies that the liquid is boiling more violently than at the previous temperature. The boiling creates a fizz which makes the drop appear whiter and more opaque.

Figure 7: Ethanol droplet impacts at 190°F.

Figure 8 shows the ethanol droplet on a 200°F surface. Compared to the previous chronology, the sharp white outlines show that the drop forms a much thinner film on the surface. The liquid also boils off much faster than at 190°F because it forms more discrete spots by the final frame.

Figure 8: Ethanol droplet impacts at 200°F.

Figure 9 shows the last set of frames for an ethanol droplet at 210°F. After landing, the drop immediately contracts into marble-like beads. The shine off the drops in the final frame shows that the ethanol has retained most of its volume, just converted into a spherical shape.

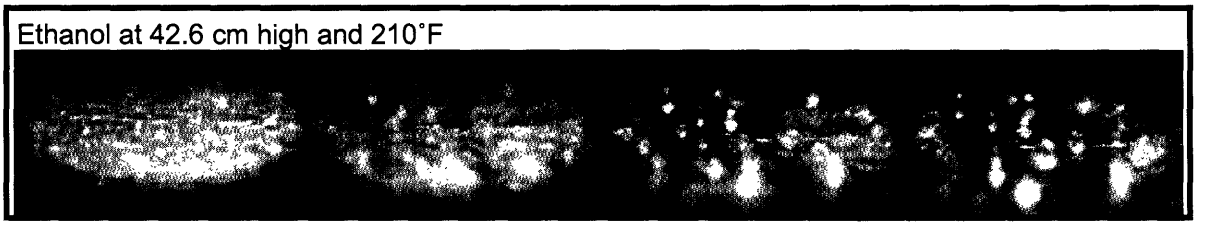

Figure 9: Ethanol droplet impacts at 210°F.

The progression from puddling to fizzing to flat film to marbling as surface temperature increases is a trend with all the other heights and liquids as well. As shown in Figure 10, the marbling effect, seen at approximately 40°F above boiling point, happens with all three fluids. To

compare the impact phenomena at other temperatures and heights, refer to Sections 8.4-8.6 for the additional chronological images.

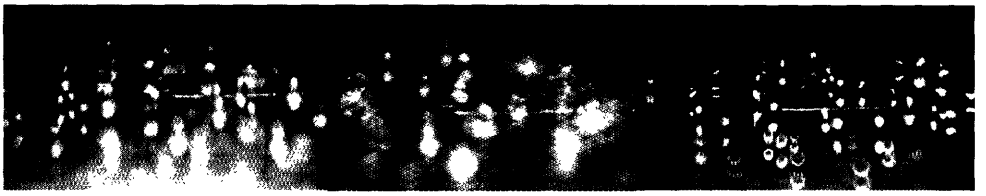

Figure 10: From left to right, drop impacts of acetone at 165°F, ethanol at 210°F, and water at 250°F.

5.2 Thermal Measurements

The experimental setup and procedure described in Sections 3.1 and 3.2 produced the tables of measurements recorded in Sections 8.1-8.3. For each fluid, the substrate temperature change from the impingement of 10 drops was recorded along with the drop frequency and visual observations of the impact. By combining these measurements with the material properties, experimental criteria, and the equations from Section 4.2, dimensionless groups were calculated for each test.

To determine which parameters in the system were relevant, first the dimensional variables were graphed against each other to study data trends. Surface temperature versus drop size resulted in vertical and horizontal clumping of data points because drop size was fixed by the syringe in use and surface temperature was held within 2°F of a chosen value. Frequency versus drop size was also inconclusive because only three drop sizes were possible from the equipment. However, graphing frequency as a function of surface temperature, as shown in Figure 11, produced a linear trend with positive slope.

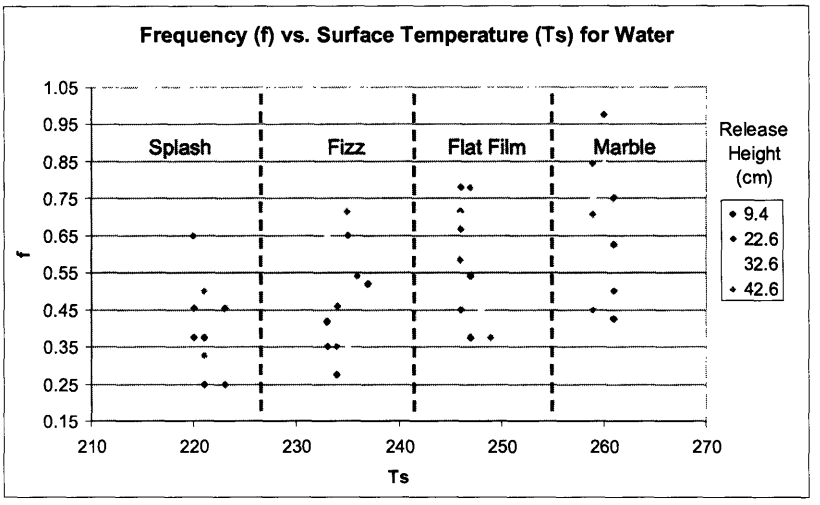

Figure 11: Frequency as a function of surface temperature (°F).

This figure shows that, at higher substrate temperatures, a higher drop rate is needed to cool the surface. This relation intuitively makes sense because hotter surfaces cause faster vaporization, so they can handle a higher volume liquid in the same time period without causing drop overlap. The graph also shows that, the higher the impact velocity, the higher the drop frequency because the drop will shatter making it easier to vaporize.

With knowledge of this linear trend present for all three fluids, the next step was to determine the dimensionless groups based on these variables. The two options for temperature were Equations 1 and 4 that both require a definition for ΔT. Assuming that the higher value is surface temperature, Ts, the other temperature could be initial liquid temperature, final surface temperature, or liquid boiling point. In these experiments, the liquids were always kept at room temperature, so that variable would be constant. As evident from the experiments, the change in surface temperature was a function of the fluid in use; i.e. water had a higher heat capacity then acetone or ethanol so its droplets caused a greater temperature decrease. This result indicated that the properties of the fluid determined its interaction with the hot surface, so boiling point which varied by fluid was chosen for the ΔT relation.

The Jacob number was chosen for the x-axis of the dimensionless graphs because, as stated above, the temperature change varied as a function of the fluid in use and Ja uses both the fluid's specific and latent heat in its definition.

With these graphs, the goal was to recognize the dimensionless groups that caused the data to converge over all fluids being tested. In this way, the graph's trends could be applied as conclusions for all liquids. Therefore in the graphical results of the experiments, all fluids are displayed and differentiated by shape. Additionally, from the high-speed photography, different impact phenomena appear to happen as a function of surface temperature. So, the data was colored by type of impact.

The initial graph of frequency versus Ja in Figure 12 shows a similar linearly increasing trend as f vs. Ts. The mixing of shaped points implies that the data has converged for all fluids, while the clumping of colors shows that the difference in boiling points is scaled by the other fluid properties.

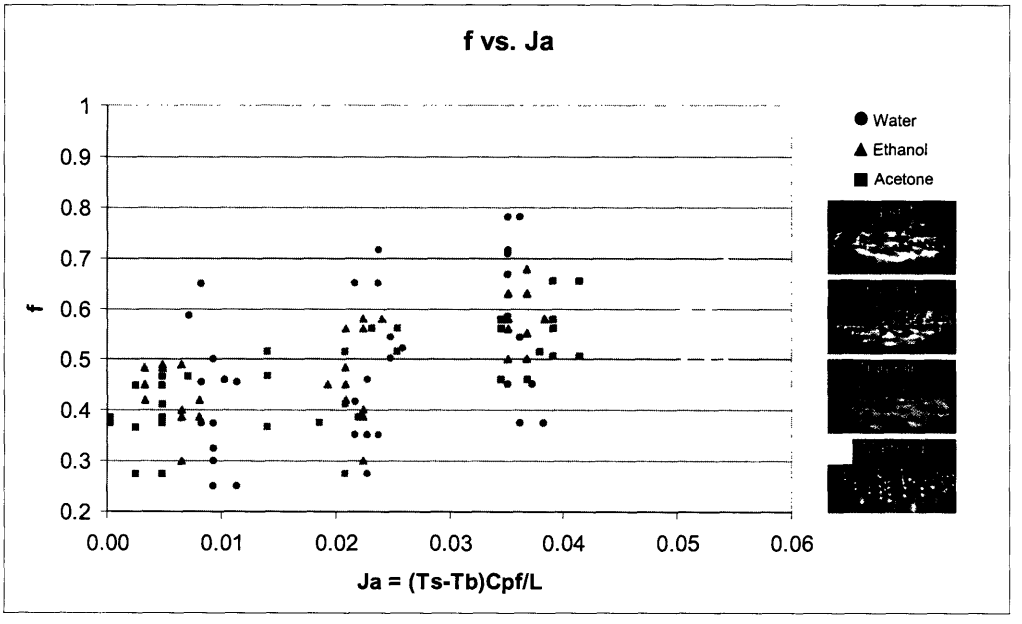

Figure 12: Frequency vs. Ja over all fluids, heights, and drop sizes.

Figure 13 takes the previous graph one step further by making the y-axis dimensionless as well using drop diameter and velocity in Equation 3. The data is again converged through intermixing of shapes, but this time displays vertical trends of impact phenomena. Since frequency increases linearly over this range, velocity must increase or the diameter decrease to create the vertical patches of color.

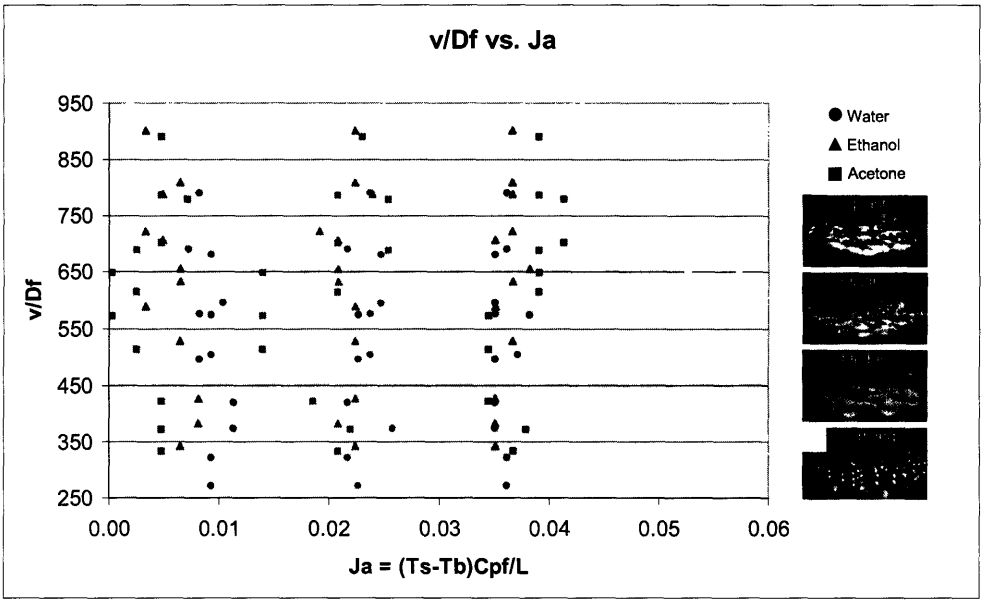

Figure 13: Graph of dimensionless drop parameters as a function of thermal properties.

Figure 14 also formed a dimensionless y-axis from the Weber number of Equation 6 and the knowledge that the increase in velocity relates to increase in frequency. As shown in the graph, the data exhibits the same trend of vertical colors and converged fluids as Figure 13. This pattern shows that the surface tension, which influenced drop size, also affects the drop's ability to evaporate from the surface.

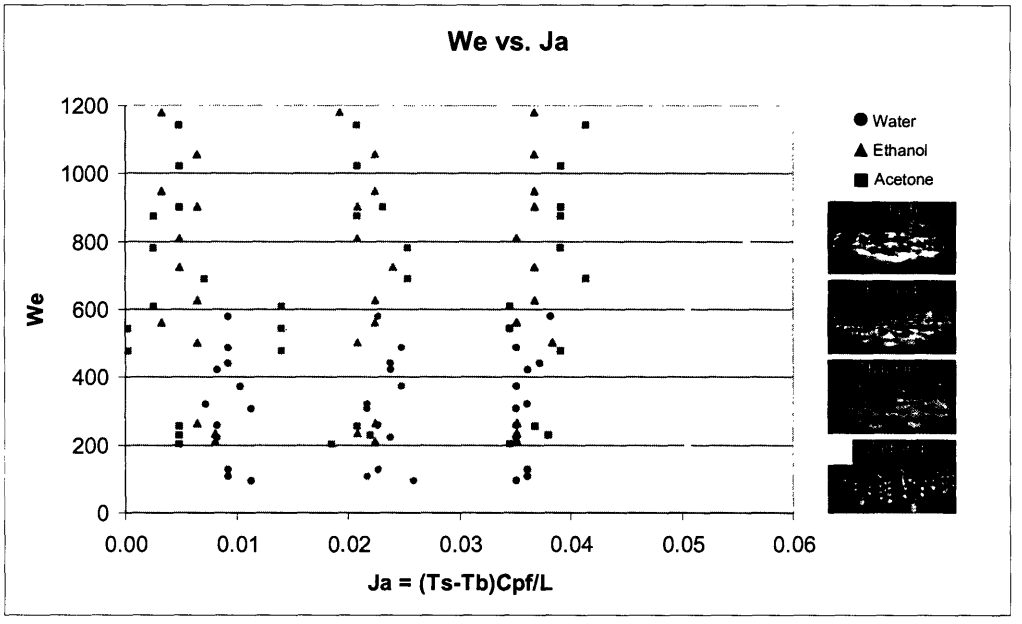

Figure 14: Graph of Weber number as a function of Jacob number over all fluids and heights.

6.0 Discussion

6.1 Analysis of High-Speed Photos

The ethanol impacts shown in Figures 6-9 clearly show the boiling evolution of the drops as a function of surface temperature. The puddling at 180°F indicates that the surface is not hot enough to rapidly initiate liquid boiling. The drop will sit on the surface as a spot of liquid for a waiting period before light boiling starts. To the naked eye, the drop radius simply decreases without much perturbation until it disappears entirely.

The second set of photos at 190°F shows an increase in the boiling to the fizzing state where ripples of boiling ruin the fluid's transparency. The drops at this stage are boiling away faster, but still have a liquid portion allowing for a heat increase.

The flat film formation at 200°F lasts for very few frames implying that this phenomenon indicates the temperature causing the quickest evaporation rate. The fluid spreads very thinly on

the surface so that the hot base interacts with the largest surface area. While boiling away, these films spray a fine mist above the impact surface.

Finally, the frames at 210°F show the transition to the marbling effect where the fluid barely contacts the plate surface. Immediately after the surface collision, the drop shatters into many smaller particles that roll across the hot surface. The mist from previous collisions and the minimal contact of these drops produces a vapor layer on the substrate surface that hinders further drop evaporation. The temperature of the plate changes very little under this phenomenon because the drops have little chance to evaporate away the heat.

Since all of the experimental fluids experienced similar transitions, it is implied that there is an optimal temperature and drop size within the flat film regime that will optimize the evaporative cooling of the plate. The other notable discovery was that the transition between phenomena happened at different intervals. While ethanol changed interaction at approximately 10°F gaps, the temperature gaps for acetone were around 5-7°F and for water around 13-15°F. This temperature spread was discovered by continually dropping a low flow rate of each fluid's drops on the substrate surface while allowing the temperature to climb and observing the temperatures where the impacts transitioned. The line between splashing and fizzing was a little hard to discern, but the fizzing to flat was more obvious and the flat to marble instantaneous.

6.2 Analysis of Graphical Relations

The linearly increasing trend of frequency versus Jacob number in Figure 12 implies that higher plate temperatures can handle a higher volume of impacting fluid in a set period. Since the fluid is vaporized up to its maximum rate in the flat film regime, there is a limit on the maximum

frequency as well since high rates in the marbling range merely result in sporadic collisions instead of increased heat removal efficiency.

The vertical patterns of data in Figures 13 and 14 are the most applicable outcomes of this experiment. The graphs can serve three purposes in designing a system for evaporative cooling. First, if the temperature of the device that needs to be cooled and the type of boiling required are known, both graphs will tell you the relation between the droplet parameters (velocity, frequency, density, surface tension, diameter) that you should use. Second, if you know the fluid you want to spray, your limitations on frequency, velocity, and diameter, and the type of boiling, you know what range of surface temperatures you can cool effectively without drop overlap or evaporation gap time. Finally, if you know the surface temperature and drop parameters, you can predict the type of boiling that will occur on the substrate surface so that you can determine the efficiency of your system in removing the heat through evaporative cooling.

The implication of these constraints is visualized in Figure 15. When designing evaporative cooling, you should choose parameters that cause the system to fall within the boxed in area. To the right, marbling occurs, reducing your heat removal; to the left, the boiling process is slow and drops overlap. The boxed area represents the range of minimum evaporation time and maximum heat transfer.

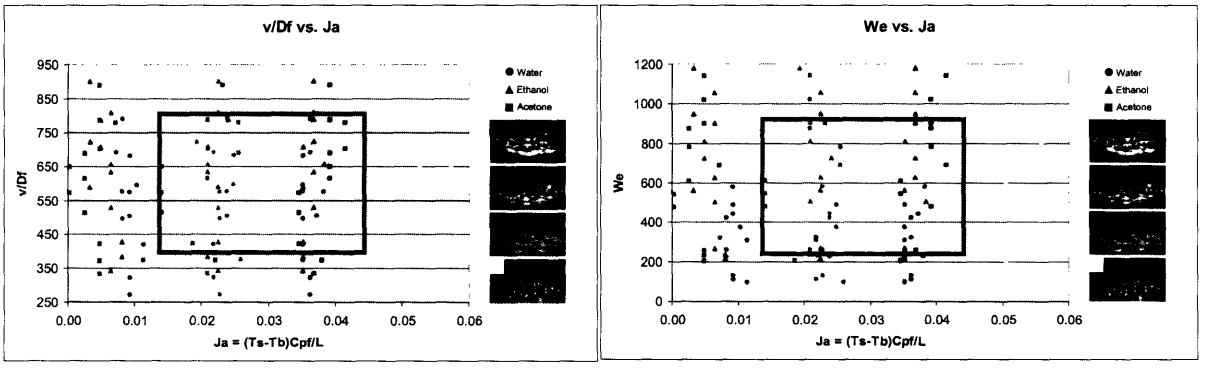

Figure 15: Design range for maximum system efficiency.

7.0 Conclusions

In conclusion, this experiment has used high-speed photography to successfully identify and visually record the progression of acetone, ethanol, and water droplet boiling on a heated copper substrate. Knowledge of these transitions combined with experimental findings led to the development of dimensionless relations between the substrate heating, fluid properties, and droplet parameters. Ignoring the interference of surface vapor layers, these dimensionless graphs allow for the design of an efficient evaporative cooling system around constrained variables.

8.0 Appendices

8.1 Acetone Data

Type	Tb	σ	ρ	μ	L	cp	k
Units	°C	N/m	kg/m³	kg/ms	J/kg	J/kg K	W/m K
Acetone	56.6	0.0238	789.9	3.89E-04	5.18E+05	2130	0.161

Height (cm)	Syringe	drops/mL	diam (mm)	mL/min	Voltage	Ts (°F)	Tf (°F)	Initial Observation
9.5	25G	56	3.24	0.400	17.00	136	134	break in half & flash fizz
9.5	20G	38.5	3.67	0.600	17.00	136	131	lump in middle with fringe
9.5	16G	27.5	4.11	0.600	17.00	136	129	lump in middle with fringe
9.5	25G	56	3.24	0.400	18.00	142	139	fizz/evap
9.5	20G	38.5	3.67	0.600	18.00	143.5	137.5	break, fizz, evap
9.5	16G	27.5	4.11	0.600	18.00	143	136.5	break, fizz, evap
9.5	25G	56	3.24	0.600	19.00	149	145	white fizz
9.5	20G	38.5	3.67	0.800	19.00	150.5	145	immediate white fizz
9.5	16G	27.5	4.11	1.000	19.00	150	143	immediate white fizz
9.5	25G	56	3.24	0.700	20.00	156	153	bead and evap, roll off edge
9.5	20G	38.5	3.67	1.000	20.00	156	150.5	minimal bead and evap
9.5	16G	27.5	4.11	1.200	20.00	159	153	white beads with evap
22.6	25G	56	3.24	0.400	17.00	134	129	splatter then evap, break into parts
22.6	20G	38.5	3.67	0.600	17.00	134	129	splatter and fizz
22.6	16G	27.5	4.11	0.600	17.00	135	130	splatter and fizz, small drops
22.6	25G	56	3.24	0.500	18.00	140	137.5	splatter & flatten
22.6	20G	38.5	3.67	0.800	18.00	140	136	splatter & fizz, bubble
22.6	16G	27.5	4.11	0.800	18.00	140	135	fizz on impact, large radius
22.6	25G	56	3.24	0.600	19.00	151	149	immediate white fizz
22.6	20G	38.5	3.67	0.900	19.00	149	146	white fizz, vapor splash
22.6	16G	27.5	4.11	1.000	19.00	149	144	white fizz, vapor splash, wide diam
22.6	25G	56	3.24	0.700	20.00	159	157	tiny marbles, evap before edge
22.6	20G	38.5	3.67	0.900	20.00	156	152	tiny marbles
22.6	16G	27.5	4.11	1.000	20.00	156	150.5	marbles and mist
32.6	25G	56	3.24	0.500	17.00	137	135	splatter into many white & clear drops
32.6	20G	38.5	3.67	0.700	17.00	135	130.5	cluster splatter, fizz
32.6	16G	27.5	4.11	0.800	17.00	135	129	cluster splatter
32.6	25G	56	3.24	0.600	18.00	145	143.5	flat scatter, white fizz
32.6	20G	38.5	3.67	0.800	18.00	145	140.5	clear liquid splatter
32.6	16G	27.5	4.11	0.900	18.00	143	136	wide splatter
32.6	25G	56	3.24	0.700	19.00	152	149	immediate mist & spray
32.6	20G	38.5	3.67	0.900	19.00	151	145.5	mist, large white spots
32.6	16G	27.5	4.11	1.100	19.00	151	144.5	mist, large white spots
32.6	25G	56	3.24	0.900	20.00	156	154	immediate vapor, tiny marbles
32.6	20G	38.5	3.67	1.100	20.00	157	152.5	tiny clear then white marbles
32.6	16G	27.5	4.11	1.300	20.00	156	151.5	same s 20G, wide coverage
42.6	25G	56	3.24	0.500	17.00	136	133	many drops
42.6	20G	38.5	3.67	0.700	17.00	136	131	flat clear and white drops
42.6	16G	27.5	4.11	0.900	17.00	136	130	flat clear and white drops
42.6	25G	56	3.24	0.600	18.00	144	141	flash vaporize
42.6	20G	38.5	3.67	0.800	18.00	143	139	wet splatter, white & clear spots
42.6	16G	27.5	4.11	0.900	18.00	143	138	wet splatter
42.6	25G	56	3.24	0.700	19.00	151	149	loud fizz, white splatter
42.6	20G	38.5	3.67	0.900	19.00	151	147	white spray, misting
42.6	16G	27.5	4.11	1.100	19.00	152	146	wide scatter of white, flat spray
42.6	25G	56	3.24	0.900	20.00	156.5	154	thud hit with mist spray marbles
42.6	20G	38.5	3.67	1.100	20.00	156	152.5	mist off surface, marble scatter
42.6	16G	27.5	4.11	1.300	20.00	157	150.5	mist jumps from surface, white spots

	Type	Tm	α	cp	k	ρ
	Units	°C	10^-6/°C	J/kg K	W/m K	kg/m³
	Copper	1083.4	16.6-17.6	390	410	2600

Height	Sgringe	Ja (Cps)	v	We	f	v/Df	v^2/L	ΔT/Ts	Re	TsCps/L	ΔTCp/L
9.5	25G	8.37E-04	1.37	200.61	0.37	420.99	3.60E-06	5.94E-03	8.99E+03	4.35E-02	4.84E-03
9.5	20G	2.09E-03	1.37	227.30	0.39	371.56	3.60E-06	1.48E-02	1.02E+04	4.35E-02	4.84E-03
9.5	16G	2.93E-03	1.37	254.28	0.28	332.14	3.60E-06	2.08E-02	1.14E+04	4.35E-02	4.84E-03
9.5	25G	1.25E-03	1.37	200.61	0.37	420.99	3.60E-06	8.42E-03	8.99E+03	4.60E-02	1.85E-02
9.5	20G	2.51E-03	1.37	227.30	0.39	371.56	3.60E-06	1.66E-02	1.02E+04	4.66E-02	2.20E-02
9.5	16G	2.72E-03	1.37	254.28	0.28	332.14	3.60E-06	1.81E-02	1.14E+04	4.64E-02	2.08E-02
9.5	25G	1.67E-03	1.37	200.61	0.56	420.99	3.60E-06	1.06E-02	8.99E+03	4.89E-02	3.45E-02
9.5	20G	2.30E-03	1.37	227.30	0.51	371.56	3.60E-06	1.43E-02	1.02E+04	4.96E-02	3.80E-02
9.5	16G	2.93E-03	1.37	254.28	0.46	332.14	3.60E-06	1.83E-02	1.14E+04	4.94E-02	3.68E-02
9.5	25G	1.25E-03	1.37	200.61	0.65	420.99	3.60E-06	7.47E-03	8.99E+03	5.19E-02	5.05E-02
9.5	20G	2.30E-03	1.37	227.30	0.64	371.56	3.60E-06	1.37E-02	1.02E+04	5.19E-02	5.05E-02
9.5	16G	2.51E-03	1.37	254.28	0.55	332.14	3.60E-06	1.46E-02	1.14E+04	5.31E-02	5.74E-02
22.6	25G	2.09E-03	2.11	477.24	0.37	649.33	8.56E-06	1.51E-02	1.39E+04	4.27E-02	2.74E-04
22.6	20G	2.09E-03	2.11	540.73	0.39	573.09	8.56E-06	1.51E-02	1.57E+04	4.27E-02	2.74E-04
22.6	16G	2.09E-03	2.11	604.91	0.28	512.29	8.56E-06	1.50E-02	1.76E+04	4.31E-02	2.56E-03
22.6	25G	1.05E-03	2.11	477.24	0.47	649.33	8.56E-06	7.14E-03	1.39E+04	4.52E-02	1.40E-02
22.6	20G	1.67E-03	2.11	540.73	0.51	573.09	8.56E-06	1.14E-02	1.57E+04	4.52E-02	1.40E-02
22.6	16G	2.09E-03	2.11	604.91	0.37	512.29	8.56E-06	1.43E-02	1.76E+04	4.52E-02	1.40E-02
22.6	25G	8.37E-04	2.11	477.24	0.56	649.33	8.56E-06	5.19E-03	1.39E+04	4.98E-02	3.91E-02
22.6	20G	1.25E-03	2.11	540.73	0.58	573.09	8.56E-06	7.91E-03	1.57E+04	4.89E-02	3.45E-02
22.6	16G	2.09E-03	2.11	604.91	0.46	512.29	8.56E-06	1.32E-02	1.76E+04	4.89E-02	3.45E-02
22.6	25G	8.37E-04	2.11	477.24	0.65	649.33	8.56E-06	4.86E-03	1.39E+04	5.31E-02	5.74E-02
22.6	20G	1.67E-03	2.11	540.73	0.58	573.09	8.56E-06	9.96E-03	1.57E+04	5.19E-02	5.05E-02
22.6	16G	2.30E-03	2.11	604.91	0.46	512.29	8.56E-06	1.37E-02	1.76E+04	5.19E-02	5.05E-02
32.6	25G	8.37E-04	2.53	688.41	0.47	779.87	1.23E-05	5.88E-03	1.67E+04	4.39E-02	7.13E-03
32.6	20G	1.88E-03	2.53	780.00	0.45	688.30	1.23E-05	1.35E-02	1.89E+04	4.31E-02	2.56E-03
32.6	16G	2.51E-03	2.53	872.57	0.37	615.27	1.23E-05	1.80E-02	2.11E+04	4.31E-02	2.56E-03
32.6	25G	6.27E-04	2.53	688.41	0.56	779.87	1.23E-05	4.10E-03	1.67E+04	4.73E-02	2.54E-02
32.6	20G	1.88E-03	2.53	780.00	0.51	688.30	1.23E-05	1.23E-02	1.89E+04	4.73E-02	2.54E-02
32.6	16G	2.93E-03	2.53	872.57	0.41	615.27	1.23E-05	1.95E-02	2.11E+04	4.64E-02	2.08E-02
32.6	25G	1.25E-03	2.53	688.41	0.65	779.87	1.23E-05	7.72E-03	1.67E+04	5.02E-02	4.14E-02
32.6	20G	2.30E-03	2.53	780.00	0.58	688.30	1.23E-05	1.43E-02	1.89E+04	4.98E-02	3.91E-02
32.6	16G	2.72E-03	2.53	872.57	0.50	615.27	1.23E-05	1.69E-02	2.11E+04	4.98E-02	3.91E-02
32.6	25G	8.37E-04	2.53	688.41	0.84	779.87	1.23E-05	4.98E-03	1.67E+04	5.19E-02	5.05E-02
32.6	20G	1.88E-03	2.53	780.00	0.71	688.30	1.23E-05	1.11E-02	1.89E+04	5.23E-02	5.28E-02
32.6	16G	1.88E-03	2.53	872.57	0.60	615.27	1.23E-05	1.12E-02	2.11E+04	5.19E-02	5.05E-02
42.6	25G	1.25E-03	2.89	899.58	0.47	891.49	1.61E-05	8.90E-03	1.90E+04	4.35E-02	4.84E-03
42.6	20G	2.09E-03	2.89	1019.26	0.45	786.82	1.61E-05	1.48E-02	2.16E+04	4.35E-02	4.84E-03
42.6	16G	2.51E-03	2.89	1140.23	0.41	703.34	1.61E-05	1.78E-02	2.41E+04	4.35E-02	4.84E-03
42.6	25G	1.25E-03	2.89	899.58	0.56	891.49	1.61E-05	8.27E-03	1.90E+04	4.68E-02	2.31E-02
42.6	20G	1.67E-03	2.89	1019.26	0.51	786.82	1.61E-05	1.11E-02	2.16E+04	4.64E-02	2.08E-02
42.6	16G	2.09E-03	2.89	1140.23	0.41	703.34	1.61E-05	1.39E-02	2.41E+04	4.64E-02	2.08E-02
42.6	25G	8.37E-04	2.89	899.58	0.65	891.49	1.61E-05	5.19E-03	1.90E+04	4.98E-02	3.91E-02
42.6	20G	1.67E-03	2.89	1019.26	0.58	786.82	1.61E-05	1.04E-02	2.16E+04	4.98E-02	3.91E-02
42.6	16G	2.51E-03	2.89	1140.23	0.50	703.34	1.61E-05	1.54E-02	2.41E+04	5.02E-02	4.14E-02
42.6	25G	1.05E-03	2.89	899.58	0.84	891.49	1.61E-05	6.20E-03	1.90E+04	5.21E-02	5.17E-02
42.6	20G	1.46E-03	2.89	1019.26	0.71	786.82	1.61E-05	8.71E-03	2.16E+04	5.19E-02	5.05E-02
42.6	16G	2.72E-03	2.89	1140.23	0.60	703.34	1.61E-05	1.60E-02	2.41E+04	5.23E-02	5.28E-02

8.2 Ethanol Data

Type	Tb	σ	ρ	μ	L	cp	k
Units	°C	N/m	kg/m³	kg/ms	J/kg	J/kg K	W/m K
Ethanol	78.29	0.0223	789	1.20E-03	8.38E+05	2400	0.169

Height (cm)	Syringe	drops/mL	diam(mm)	mL/min	Voltage	Ts (°F)	Tf (°F)	Initial Observation
9.5	25G	58	3.21	0.400	19.00	178	174.5	splash down as water
9.5	20G	42	3.57	0.600	19.00	178	172	large water puddle
9.5	16G	30	3.99	0.600	19.00	177	171	bounce back off plate, liquid puddle
9.5	25G	58	3.21	0.400	20.00	187	182	single splat in middle, bubbling
9.5	20G	42	3.57	0.600	20.00	186	180	single splat in middle, bubbling
9.5	16G	30	3.99	0.600	20.00	187	179	flatten and bubble as single
9.5	25G	58	3.21	0.600	21.00	195	190	small radius on drop, flatten
9.5	20G	42	3.57	0.800	21.00	195	188	single landing of white fizz
9.5	16G	30	3.99	1.000	21.00	195	184.5	flat white splatter
9.5	25G	58	3.21	0.700	22.00	205	199	small impact radius, immediate vapor
9.5	20G	42	3.57	1.000	22.00	207	202	lands as beads
9.5	16G	30	3.99	1.200	22.00	205	195	lands as beads and slightly roll
22.6	25G	58	3.21	0.400	19.00	177	174	land as single liquid spot
22.6	20G	42	3.57	0.600	19.00	175	171	drop slides on surface
22.6	16G	30	3.99	0.600	19.00	177	171	flat pool on surface
22.6	25G	58	3.21	0.500	20.00	186	183	flat landing, small bubbles in spot
22.6	20G	42	3.57	0.800	20.00	187	182	flat, bubbled landing
22.6	16G	30	3.99	0.800	20.00	187	179	clear liquid with white bubbles
22.6	25G	58	3.21	0.600	20.50	197	193	immediate flattening
22.6	20G	42	3.57	0.900	20.50	195	188	slight overlap of drops, thin film
22.6	16G	30	3.99	1.000	20.50	196	187	splatter of tiny shards on impact
22.6	25G	58	3.21	0.700	21.00	206	200.5	tiny drops vaporize on contact
22.6	20G	42	3.57	0.900	21.00	205	198	drops break on impact
22.6	16G	30	3.99	1.000	21.00	207	197	drops break on impact
32.6	25G	58	3.21	0.500	20.00	176	171.5	drop broke into parts on impact
32.6	20G	42	3.57	0.700	20.00	176	171	liquid pooling
32.6	16G	30	3.99	0.800	20.00	177	168	liquid pooling
32.6	25G	58	3.21	0.600	20.50	188	182.5	film bubbling on impact
32.6	20G	42	3.57	0.800	20.50	186	180	drop separates and rejoins
32.6	16G	30	3.99	0.900	20.50	186	176	single hzy liquid spot, waves of boil
32.6	25G	58	3.21	0.700	21.00	196	191	breaks into drops, flat fizz
32.6	20G	42	3.57	0.900	21.00	195	189	breaks into fizzing drops, mist
32.6	16G	30	3.99	1.100	21.00	196	187	flat fizzing layer
32.6	25G	58	3.21	0.900	22.00	207	203	breaks into small marbles
32.6	20G	42	3.57	1.100	22.00	208	202	breaks into small marbles
32.6	16G	30	3.99	1.300	22.00	207	198	marbles become flat splatters
42.6	25G	58	3.21	0.500	20.00	175	172	multiple flat splatters
42.6	20G	42	3.57	0.700	20.00	177	172	splats into small pools
42.6	16G	30	3.99	0.900	20.00	175	168.5	some drop overlap, pooling
42.6	25G	58	3.21	0.600	20.50	187	182	one spot of fizzing liquid
42.6	20G	42	3.57	0.800	20.50	187	180	multiple fizzing drops
42.6	16G	30	3.99	0.900	20.50	185	177	multiple fizzing drops
42.6	25G	58	3.21	0.700	21.00	196	191	multiple films of fizz
42.6	20G	42	3.57	0.900	21.00	196	189	multiple drops spread out, misting
42.6	16G	30	3.99	1.100	21.00	196	186	flat films of fizzing liquid
42.6	25G	58	3.21	0.900	22.00	206	202.5	tiny marble drops
42.6	20G	42	3.57	1.100	22.00	206	200	tiny drops in flower pattern at center
42.6	16G	30	3.99	1.300	22.00	207	200	marbles rolled off edge

	Type	Tm	α	cp	k	ρ
	Units	°C	10^-6/°C	J/kg K	W/m K	kg/m³
	Copper	1083.4	16.6-17.6	390	410	2600

Height	Sgringe	Ja (Cps)	v	We	f	v/Df	v^2/L	ΔT/Ts	Re	TsCps/L	ΔTCp/L
9.5	25G	9.05E-04	1.37	211.37	0.39	425.94	2.22E-06	7.40E-03	2.88E+03	3.77E-02	8.08E-03
9.5	20G	1.55E-03	1.37	235.38	0.42	382.50	2.22E-06	1.27E-02	3.20E+03	3.77E-02	8.08E-03
9.5	16G	1.55E-03	1.37	263.32	0.30	341.91	2.22E-06	1.28E-02	3.58E+03	3.75E-02	6.49E-03
9.5	25G	1.29E-03	1.37	211.37	0.39	425.94	2.22E-06	9.96E-03	2.88E+03	4.01E-02	2.24E-02
9.5	20G	1.55E-03	1.37	235.38	0.42	382.50	2.22E-06	1.20E-02	3.20E+03	3.98E-02	2.08E-02
9.5	16G	2.07E-03	1.37	263.32	0.30	341.91	2.22E-06	1.59E-02	3.58E+03	4.01E-02	2.24E-02
9.5	25G	1.29E-03	1.37	211.37	0.58	425.94	2.22E-06	9.47E-03	2.88E+03	4.21E-02	3.51E-02
9.5	20G	1.81E-03	1.37	235.38	0.56	382.50	2.22E-06	1.33E-02	3.20E+03	4.21E-02	3.51E-02
9.5	16G	2.71E-03	1.37	263.32	0.50	341.91	2.22E-06	1.99E-02	3.58E+03	4.21E-02	3.51E-02
9.5	25G	1.55E-03	1.37	211.37	0.68	425.94	2.22E-06	1.07E-02	2.88E+03	4.47E-02	5.10E-02
9.5	20G	1.29E-03	1.37	235.38	0.70	382.50	2.22E-06	8.82E-03	3.20E+03	4.52E-02	5.42E-02
9.5	16G	2.59E-03	1.37	263.32	0.60	341.91	2.22E-06	1.78E-02	3.58E+03	4.47E-02	5.10E-02
22.6	25G	7.76E-04	2.11	502.85	0.39	656.97	5.29E-06	6.39E-03	4.44E+03	3.75E-02	6.49E-03
22.6	20G	1.03E-03	2.11	559.97	0.42	589.96	5.29E-06	8.63E-03	4.94E+03	3.70E-02	3.31E-03
22.6	16G	1.55E-03	2.11	626.43	0.30	527.36	5.29E-06	1.28E-02	5.53E+03	3.75E-02	6.49E-03
22.6	25G	7.76E-04	2.11	502.85	0.48	656.97	5.29E-06	6.01E-03	4.44E+03	3.98E-02	2.08E-02
22.6	20G	1.29E-03	2.11	559.97	0.56	589.96	5.29E-06	9.96E-03	4.94E+03	4.01E-02	2.24E-02
22.6	16G	2.07E-03	2.11	626.43	0.40	527.36	5.29E-06	1.59E-02	5.53E+03	4.01E-02	2.24E-02
22.6	25G	1.03E-03	2.11	502.85	0.58	656.97	5.29E-06	7.48E-03	4.44E+03	4.27E-02	3.83E-02
22.6	20G	1.81E-03	2.11	559.97	0.63	589.96	5.29E-06	1.33E-02	4.94E+03	4.21E-02	3.51E-02
22.6	16G	2.33E-03	2.11	626.43	0.50	527.36	5.29E-06	1.69E-02	5.53E+03	4.24E-02	3.67E-02
22.6	25G	1.42E-03	2.11	502.85	0.68	656.97	5.29E-06	9.76E-03	4.44E+03	4.50E-02	5.26E-02
22.6	20G	1.81E-03	2.11	559.97	0.63	589.96	5.29E-06	1.25E-02	4.94E+03	4.47E-02	5.10E-02
22.6	16G	2.59E-03	2.11	626.43	0.50	527.36	5.29E-06	1.76E-02	5.53E+03	4.52E-02	5.42E-02
32.6	25G	1.16E-03	2.53	725.35	0.48	789.04	7.63E-06	9.65E-03	5.33E+03	3.72E-02	4.90E-03
32.6	20G	1.29E-03	2.53	807.74	0.49	708.56	7.63E-06	1.07E-02	5.94E+03	3.72E-02	4.90E-03
32.6	16G	2.33E-03	2.53	903.61	0.40	633.38	7.63E-06	1.92E-02	6.64E+03	3.75E-02	6.49E-03
32.6	25G	1.42E-03	2.53	725.35	0.58	789.04	7.63E-06	1.09E-02	5.33E+03	4.03E-02	2.40E-02
32.6	20G	1.55E-03	2.53	807.74	0.56	708.56	7.63E-06	1.20E-02	5.94E+03	3.98E-02	2.08E-02
32.6	16G	2.59E-03	2.53	903.61	0.45	633.38	7.63E-06	2.00E-02	6.64E+03	3.98E-02	2.08E-02
32.6	25G	1.29E-03	2.53	725.35	0.68	789.04	7.63E-06	9.41E-03	5.33E+03	4.24E-02	3.67E-02
32.6	20G	1.55E-03	2.53	807.74	0.63	708.56	7.63E-06	1.14E-02	5.94E+03	4.21E-02	3.51E-02
32.6	16G	2.33E-03	2.53	903.61	0.55	633.38	7.63E-06	1.69E-02	6.64E+03	4.24E-02	3.67E-02
32.6	25G	1.03E-03	2.53	725.35	0.87	789.04	7.63E-06	7.05E-03	5.33E+03	4.52E-02	5.42E-02
32.6	20G	1.55E-03	2.53	807.74	0.77	708.56	7.63E-06	1.05E-02	5.94E+03	4.55E-02	5.58E-02
32.6	16G	2.33E-03	2.53	903.61	0.65	633.38	7.63E-06	1.59E-02	6.64E+03	4.52E-02	5.42E-02
42.6	25G	7.76E-04	2.89	947.85	0.48	901.98	9.97E-06	6.48E-03	6.09E+03	3.70E-02	3.31E-03
42.6	20G	1.29E-03	2.89	1055.52	0.49	809.97	9.97E-06	1.06E-02	6.78E+03	3.75E-02	6.49E-03
42.6	16G	1.68E-03	2.89	1180.79	0.45	724.04	9.97E-06	1.40E-02	7.59E+03	3.70E-02	3.31E-03
42.6	25G	1.29E-03	2.89	947.85	0.58	901.98	9.97E-06	9.96E-03	6.09E+03	4.01E-02	2.24E-02
42.6	20G	1.81E-03	2.89	1055.52	0.56	809.97	9.97E-06	1.39E-02	6.78E+03	4.01E-02	2.24E-02
42.6	16G	2.07E-03	2.89	1180.79	0.45	724.04	9.97E-06	1.61E-02	7.59E+03	3.96E-02	1.92E-02
42.6	25G	1.29E-03	2.89	947.85	0.68	901.98	9.97E-06	9.41E-03	6.09E+03	4.24E-02	3.67E-02
42.6	20G	1.81E-03	2.89	1055.52	0.63	809.97	9.97E-06	1.32E-02	6.78E+03	4.24E-02	3.67E-02
42.6	16G	2.59E-03	2.89	1180.79	0.55	724.04	9.97E-06	1.88E-02	7.59E+03	4.24E-02	3.67E-02
42.6	25G	9.05E-04	2.89	947.85	0.87	901.98	9.97E-06	6.21E-03	6.09E+03	4.50E-02	5.26E-02
42.6	20G	1.55E-03	2.89	1055.52	0.77	809.97	9.97E-06	1.06E-02	6.78E+03	4.50E-02	5.26E-02
42.6	16G	1.81E-03	2.89	1180.79	0.65	724.04	9.97E-06	1.23E-02	7.59E+03	4.52E-02	5.42E-02

8.3 Water Data

Type	Tb	σ	ρ	μ	L	cp	k
Units	°C	N/m	kg/m³	kg/ms	J/kg	J/kg K	W/m K
Water	100.0	0.0728	998	1.00E-03	2.26E+06	4200	0.607

Height (cm)	Syringe	drop/mL	diam (mm)	mL/min	Voltage	Ts (°F)	Tf(°F)	Initial Observation
9.5	25G	39	3.66	0.700	23.00	223	207.5	lands as single drop, sprays shards
9.5	20G	25	4.24	0.900	23.00	221	194	land as blob and evap off quickly
9.5	16G	15	5.03	1.000	23.00	221	190	drops rapid evap, quick bubbling
9.5	25G	39	3.66	0.800	24.00	237	221	immediate drop flattening and evap
9.5	20G	25	4.24	1.000	24.00	233	208	spraying off little shards as quickly evap
9.5	16G	15	5.03	1.100	24.00	234	196	spraying of mist and little drops
9.5	25G	39	3.66	1.100	25.00	246	229	very quick evap with associated spray
9.5	20G	25	4.24	1.300	25.00	247	220.5	quick drop evaporating
9.5	16G	15	5.03	1.500	25.00	247	208	lands and then spray flies up
9.5	25G	39	3.66	1.300	26.00	260	245	spray marbles at edges, middle vaporize
9.5	20G	25	4.24	1.500	26.00	261	234	spray marbles at edges, middle vaporize
9.5	16G	15	5.03	1.700	26.00	261	218	loud fizzing sound as drop evap
22.6	25G	39	3.66	0.700	23.00	220	205	land as single drop and evap quickly
22.6	20G	25	4.24	0.900	23.00	220	192	land as wet splat, then evap
22.6	16G	15	5.03	1.000	23.00	223	187	liquid begans pooling near the end
22.6	25G	39	3.66	1.000	24.00	235	218	liquid lands as flat, wet spot
22.6	20G	25	4.24	1.100	24.00	234	204	liquid lands as flat, wet spot
22.6	16G	15	5.03	1.400	24.00	233	193	liquid lands and evaporates with gap time
22.6	25G	39	3.66	1.200	25.00	246	227	liquid lands as flat, wet spot
22.6	20G	25	4.24	1.600	25.00	246	214	flat wet spot that then evap
22.6	16G	15	5.03	1.800	25.00	246	203	gap time when evap at beginning
22.6	25G	39	3.66	1.500	26.00	260	242	drop vaporizes at middle
22.6	20G	25	4.24	1.800	26.00	261	231	immediate evap with marbles from center
22.6	16G	15	5.03	2.000	26.00	261	212	drop lands as large spot, evap quickly
32.6	25G	39	3.66	0.900	19.00	219	199	lands as wet spot
32.6	20G	25	4.24	1.100	19.00	222	194	large bubbling on surface after cooling
32.6	16G	15	5.03	1.200	19.00	221	190	pooling at bottom, last drops bounce
32.6	25G	39	3.66	1.000	20.00	233	217	wet spot on surface, some overspray
32.6	20G	25	4.24	1.200	20.00	236	209	wet spots on surface, evap before next
32.6	16G	15	5.03	1.400	20.00	235	195	drops splash into each other at end
32.6	25G	39	3.66	1.200	21.00	247	234	single drop in center then quick vapor
32.6	20G	25	4.24	1.700	21.00	246	221	water drop flatens out into wide diameter
32.6	16G	15	5.03	1.800	21.00	248	211	flat spot with overlapping as surface cools
32.6	25G	39	3.66	1.300	22.00	260	252	lands as marbles, sprays and rolls off
32.6	20G	25	4.24	1.800	22.00	259	243	marbles and sprays, forms thin single spot
32.6	16G	15	5.03	2.000	22.00	263	232	initially marbles & then becomes flat drop
42.6	25G	39	3.66	1.000	19.00	220	198	lands as single wet spot on surface
42.6	20G	25	4.24	1.200	19.00	221	191	lands as wet splat
42.6	16G	15	5.03	1.300	19.00	221	187	lands as wet splat
42.6	25G	39	3.66	1.100	20.00	235	218	wet spot then immediate evap
42.6	20G	25	4.24	1.300	20.00	236	211	wet spot then immediate evap
42.6	16G	15	5.03	1.400	20.00	234	193	wet spot then immediate evap
42.6	25G	39	3.66	1.200	21.00	247	229	flat spot that vaporizes quickly
42.6	20G	25	4.24	1.400	21.00	246	220	flat spot that vaporizes quickly
42.6	16G	15	5.03	1.500	21.00	249	210	flat spot that vaporizes quickly
42.6	25G	39	3.66	1.300	22.00	259	239	flat spot with marbles on edges
42.6	20G	25	4.24	1.700	22.00	259	226	lands as flat spot with beads on edges
42.6	16G	15	5.03	1.800	22.00	259	211	lands as flat spot with beads on edges

	Type	Tm	α	cp	k	ρ
	Units	°C	10^-6/°C	J/kg K	W/m K	kg/m³
	Copper	1083.4	16.6-17.6	390	410	2600

Height	Syringe	Ja (Cps)	v	Ve	f	v/Df	v^2/L	ΔT/Ts	Re	TsCps/L	ΔTCp/L
9.5	25G	1.49E-03	1.37	93.48	0.46	373.16	8.25E-07	2.50E-02	4.97E+03	1.83E-02	1.14E-02
9.5	20G	2.59E-03	1.37	108.42	0.38	321.75	8.25E-07	4.41E-02	5.76E+03	1.81E-02	9.30E-03
9.5	16G	2.97E-03	1.37	128.55	0.25	271.38	8.25E-07	5.06E-02	6.83E+03	1.81E-02	9.30E-03
9.5	25G	1.54E-03	1.37	93.48	0.52	373.16	8.25E-07	2.41E-02	4.97E+03	1.97E-02	2.58E-02
9.5	20G	2.40E-03	1.37	108.42	0.42	321.75	8.25E-07	3.84E-02	5.76E+03	1.93E-02	2.17E-02
9.5	16G	3.65E-03	1.37	128.55	0.28	271.38	8.25E-07	5.81E-02	6.83E+03	1.94E-02	2.27E-02
9.5	25G	1.63E-03	1.37	93.48	0.72	373.16	8.25E-07	2.45E-02	4.97E+03	2.05E-02	3.51E-02
9.5	20G	2.54E-03	1.37	108.42	0.54	321.75	8.25E-07	3.80E-02	5.76E+03	2.06E-02	3.62E-02
9.5	16G	3.74E-03	1.37	128.55	0.38	271.38	8.25E-07	5.60E-02	6.83E+03	2.06E-02	3.62E-02
9.5	25G	1.44E-03	1.37	93.48	0.85	373.16	8.25E-07	2.03E-02	4.97E+03	2.19E-02	4.96E-02
9.5	20G	2.59E-03	1.37	108.42	0.63	321.75	8.25E-07	3.64E-02	5.76E+03	2.20E-02	5.06E-02
9.5	16G	4.13E-03	1.37	128.55	0.43	271.38	8.25E-07	5.80E-02	6.83E+03	2.20E-02	5.06E-02
22.6	25G	1.44E-03	2.11	222.39	0.46	575.56	1.96E-06	2.46E-02	7.67E+03	1.80E-02	8.27E-03
22.6	20G	2.69E-03	2.11	257.93	0.38	496.27	1.96E-06	4.60E-02	8.89E+03	1.80E-02	8.27E-03
22.6	16G	3.45E-03	2.11	305.80	0.25	418.57	1.96E-06	5.82E-02	1.05E+04	1.83E-02	1.14E-02
22.6	25G	1.63E-03	2.11	222.39	0.65	575.56	1.96E-06	2.58E-02	7.67E+03	1.95E-02	2.38E-02
22.6	20G	2.88E-03	2.11	257.93	0.46	496.27	1.96E-06	4.59E-02	8.89E+03	1.94E-02	2.27E-02
22.6	16G	3.84E-03	2.11	305.80	0.35	418.57	1.96E-06	6.14E-02	1.05E+04	1.93E-02	2.17E-02
22.6	25G	1.82E-03	2.11	222.39	0.78	575.56	1.96E-06	2.74E-02	7.67E+03	2.05E-02	3.51E-02
22.6	20G	3.07E-03	2.11	257.93	0.67	496.27	1.96E-06	4.62E-02	8.89E+03	2.05E-02	3.51E-02
22.6	16G	4.13E-03	2.11	305.80	0.45	418.57	1.96E-06	6.20E-02	1.05E+04	2.05E-02	3.51E-02
22.6	25G	1.73E-03	2.11	222.39	0.98	575.56	1.96E-06	2.44E-02	7.67E+03	2.19E-02	4.96E-02
22.6	20G	2.88E-03	2.11	257.93	0.75	496.27	1.96E-06	4.04E-02	8.89E+03	2.20E-02	5.06E-02
22.6	16G	4.70E-03	2.11	305.80	0.50	418.57	1.96E-06	6.60E-02	1.05E+04	2.20E-02	5.06E-02
32.6	25G	1.92E-03	2.53	320.80	0.59	691.27	2.83E-06	3.30E-02	9.21E+03	1.79E-02	7.23E-03
32.6	20G	2.69E-03	2.53	372.05	0.46	596.03	2.83E-06	4.55E-02	1.07E+04	1.82E-02	1.03E-02
32.6	16G	2.97E-03	2.53	441.12	0.30	502.71	2.83E-06	5.06E-02	1.27E+04	1.81E-02	9.30E-03
32.6	25G	1.54E-03	2.53	320.80	0.65	691.27	2.83E-06	2.46E-02	9.21E+03	1.93E-02	2.17E-02
32.6	20G	2.59E-03	2.53	372.05	0.50	596.03	2.83E-06	4.08E-02	1.07E+04	1.96E-02	2.48E-02
32.6	16G	3.84E-03	2.53	441.12	0.35	502.71	2.83E-06	6.08E-02	1.27E+04	1.95E-02	2.38E-02
32.6	25G	1.25E-03	2.53	320.80	0.78	691.27	2.83E-06	1.87E-02	9.21E+03	2.06E-02	3.62E-02
32.6	20G	2.40E-03	2.53	372.05	0.71	596.03	2.83E-06	3.61E-02	1.07E+04	2.05E-02	3.51E-02
32.6	16G	3.55E-03	2.53	441.12	0.45	502.71	2.83E-06	5.29E-02	1.27E+04	2.07E-02	3.72E-02
32.6	25G	7.68E-04	2.53	320.80	0.85	691.27	2.83E-06	1.08E-02	9.21E+03	2.19E-02	4.96E-02
32.6	20G	1.54E-03	2.53	372.05	0.75	596.03	2.83E-06	2.18E-02	1.07E+04	2.18E-02	4.86E-02
32.6	16G	2.97E-03	2.53	441.12	0.50	502.71	2.83E-06	4.14E-02	1.27E+04	2.22E-02	5.27E-02
42.6	25G	2.11E-03	2.89	419.20	0.65	790.21	3.70E-06	3.61E-02	1.05E+04	1.80E-02	8.27E-03
42.6	20G	2.88E-03	2.89	486.18	0.50	681.35	3.70E-06	4.90E-02	1.22E+04	1.81E-02	9.30E-03
42.6	16G	3.26E-03	2.89	576.43	0.33	574.67	3.70E-06	5.55E-02	1.45E+04	1.81E-02	9.30E-03
42.6	25G	1.63E-03	2.89	419.20	0.72	790.21	3.70E-06	2.58E-02	1.05E+04	1.95E-02	2.38E-02
42.6	20G	2.40E-03	2.89	486.18	0.54	681.35	3.70E-06	3.78E-02	1.22E+04	1.96E-02	2.48E-02
42.6	16G	3.93E-03	2.89	576.43	0.35	574.67	3.70E-06	6.26E-02	1.45E+04	1.94E-02	2.27E-02
42.6	25G	1.73E-03	2.89	419.20	0.78	790.21	3.70E-06	2.58E-02	1.05E+04	2.06E-02	3.62E-02
42.6	20G	2.49E-03	2.89	486.18	0.58	681.35	3.70E-06	3.75E-02	1.22E+04	2.05E-02	3.51E-02
42.6	16G	3.74E-03	2.89	576.43	0.38	574.67	3.70E-06	5.55E-02	1.45E+04	2.08E-02	3.82E-02
42.6	25G	1.92E-03	2.89	419.20	0.85	790.21	3.70E-06	2.72E-02	1.05E+04	2.18E-02	4.86E-02
42.6	20G	3.17E-03	2.89	486.18	0.71	681.35	3.70E-06	4.49E-02	1.22E+04	2.18E-02	4.86E-02
42.6	16G	4.61E-03	2.89	576.43	0.45	574.67	3.70E-06	6.53E-02	1.45E+04	2.18E-02	4.86E-02

8.4 Acetone Drop Pictures

Acetone at 9.5 cm high and 130˚F

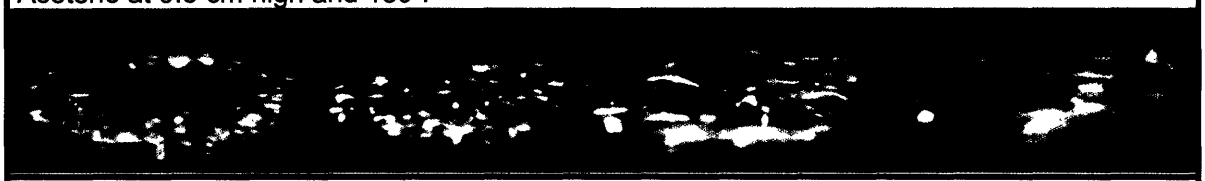

Acetone at 9.5 cm high and 140˚F

Acetone at 9.5 cm high and 150˚F

Acetone at 9.5 cm high and 160˚F

Acetone at 9.5 cm high and 170˚F

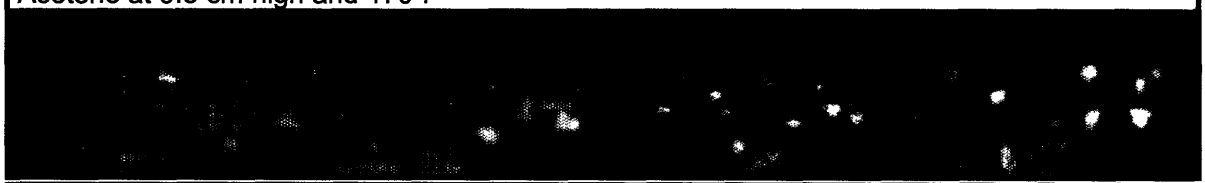

Acetone at 42.6 cm high and 135˚F

Acetone at 42.6 cm high and 145˚F

Acetone at 42.6 cm high and 155˚F

Acetone at 42.6 cm high and 165˚F

8.5 Ethanol Drop Pictures

Ethanol at 9.5 cm high and 170˚F

Ethanol at 9.5 cm high and 180˚F

Ethanol at 9.5 cm high and 190˚F

Ethanol at 9.5 cm high and 200˚F

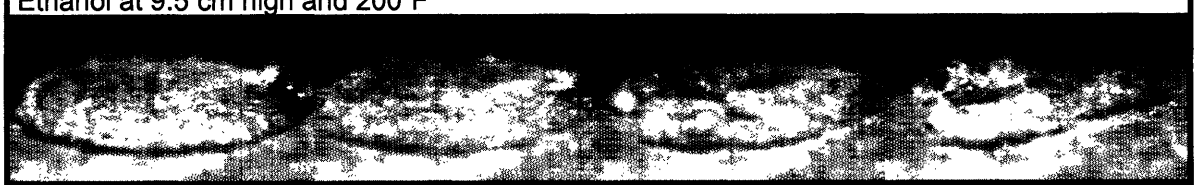

Ethanol at 9.5 cm high and 210˚F

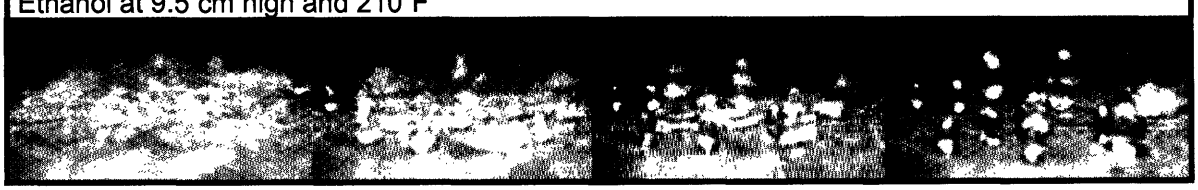

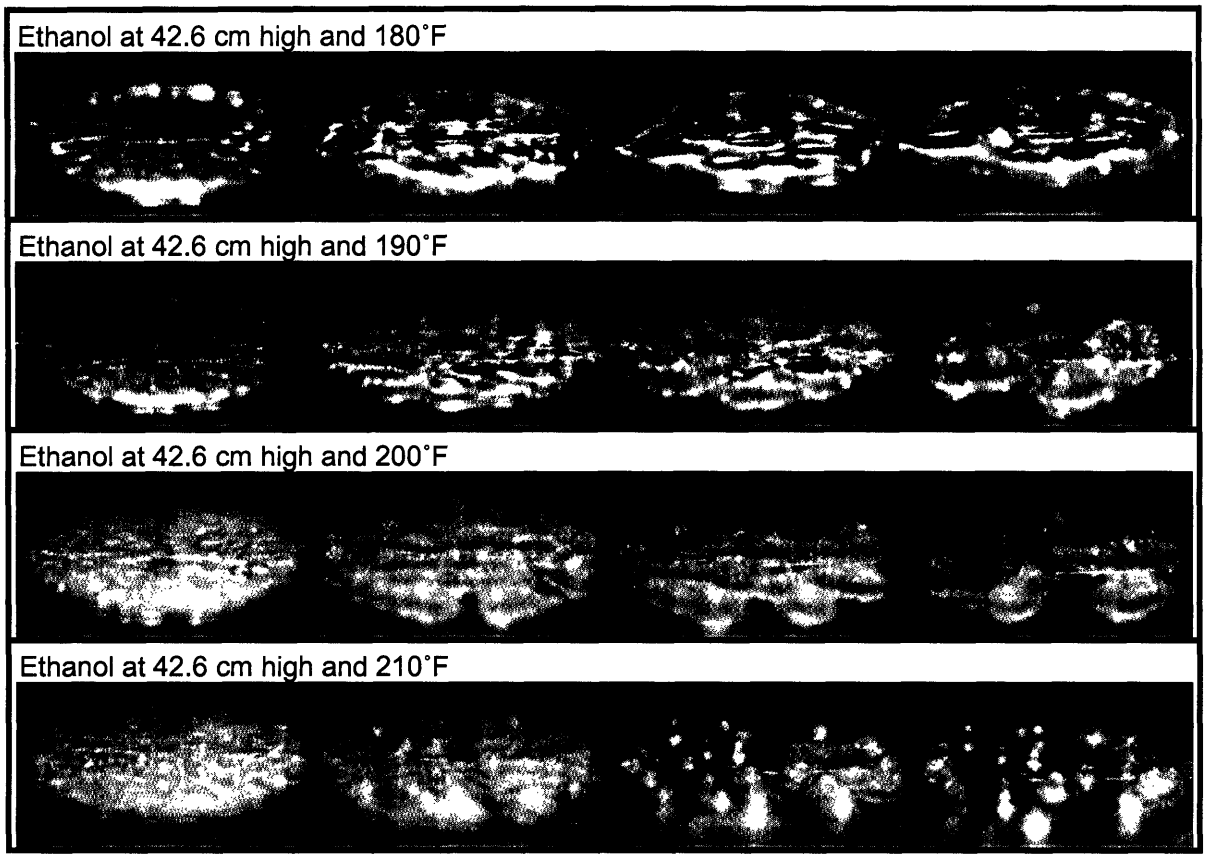

8.6 Water Drop Pictures

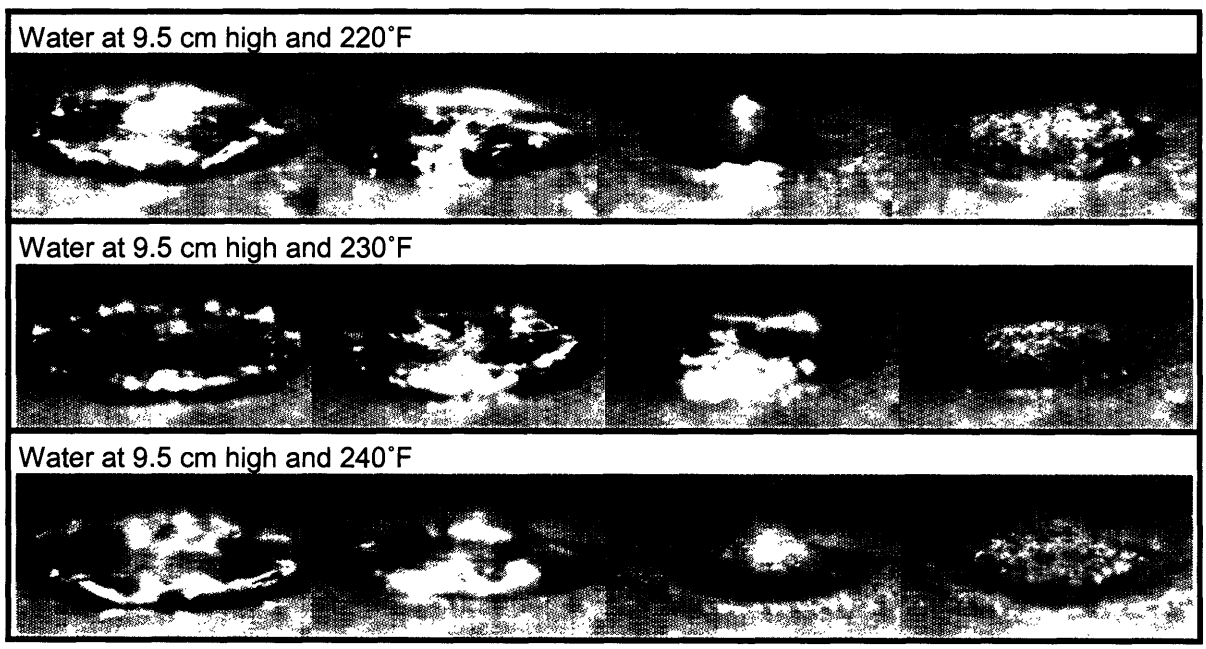

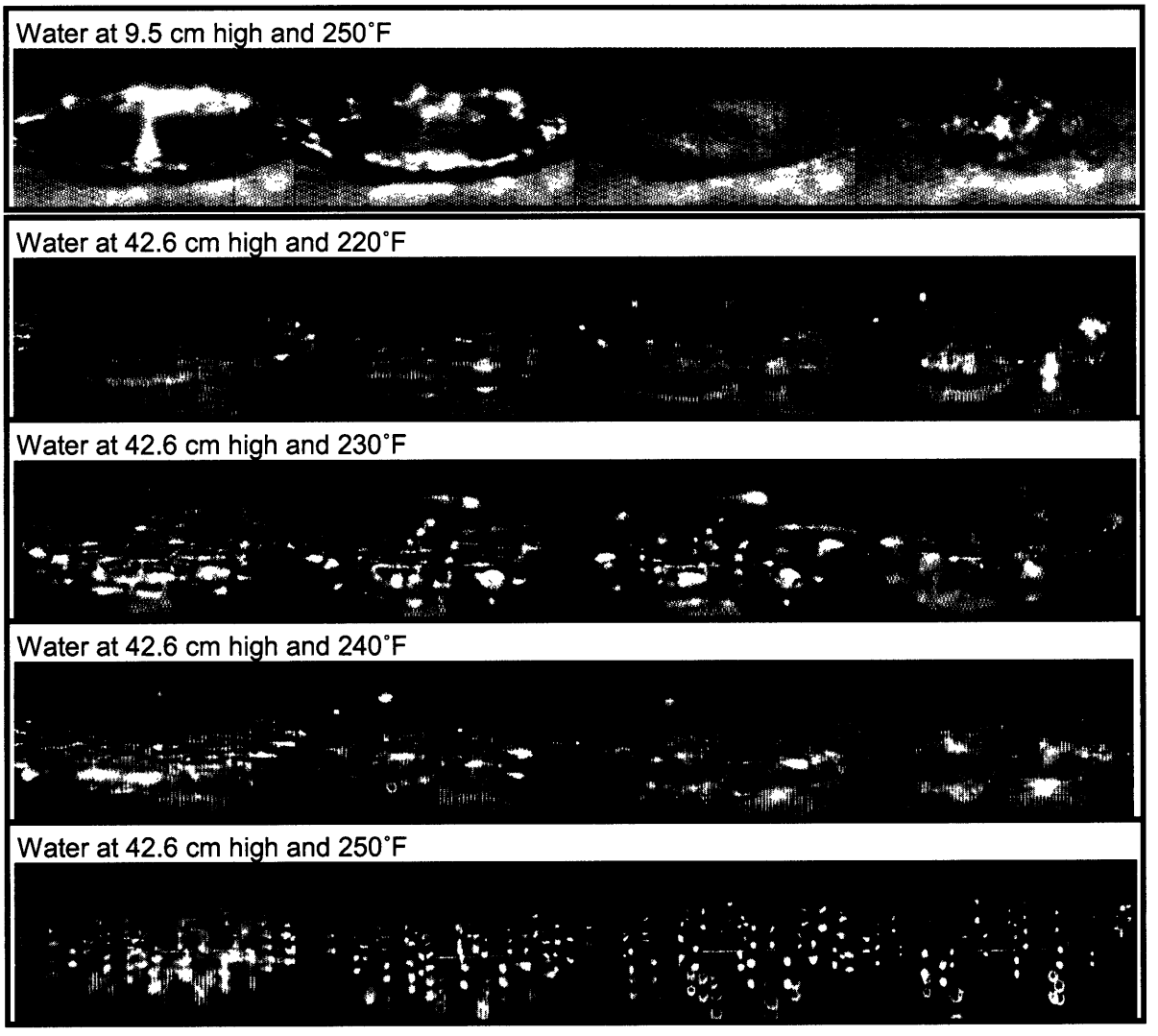
Water at 9.5 cm high and 250˚F
Water at 42.6 cm high and 220˚F
Water at 42.6 cm high and 230˚F
Water at 42.6 cm high and 240˚F
Water at 42.6 cm high and 250˚F

9.0 References

[1] S. Chandra, C.T. Avedisian, On the collision of a droplet with a solid surface, Proc. R. Soc. Lond. A 432 (1991) 13-41.

[2] K. Makino, I. Michiyoshi, The behavior of a water droplet on heater surfaces, Int. J. Heat Mass Transfer 27 (1984) 781-791.

[3] S. Inada, Y. Miyasaka, K. Sakamoto, K. Hojo, Liquid-solid contact state and fluctuation of the vapor film thickness of a drop impinging on a heated surface, J. Chem. Eng. Japan 21 (1988) 463-468.

[4] J.D. Bernardin, C.J. Stebbins, I. Mudawar, Mapping of impact and heat transfer regimes of water drops impinging on a polished surface, Int. J. Heat Mass Transfer 40 (1997) 247-267.

[5] S.S. Hsieh, T-C Fan, H-H Tsai, Spray cooling characteristics of water and R-134a; Part I: nucleate boiling, Int. J. Heat Mass Transfer 47 (2004) 5703-5712.

[6] S.S. Hsieh, T-C Fan, H-H Tsai, Spray cooling characteristics of water and R-134a; Part II: transient cooling, Int. J. Heat Mass Transfer 47 (2004) 5713-5724.

[7] A. Karl, A. Frohn, Experimental investigation of interaction processes between droplets and hot walls, Phys. Fluids 12 (2000) 785-796.

[8] W. Jia, H. Qiu, Fringe probing of an evaporating microdroplet on a hot surface, Int. J. Heat Mass Transfer 45 (2002) 4141-4150.

[9] K.J. Baumeister, F.F. Simon, Leidenfrost Temperature – Its correlation for liquid metals, cryogens, hydrocarbons, and water, ASME J. Heat Trans. (1973) 166-173.

[10] L.H.J. Wachters, N.A.J. Westerling, The heat transfer from a hot wall to impinging water drops in the spheroidal state, Chem. Eng. Sci. 21 (1966) 1047-1056.

[11] C.O. Pedersen, An experimental study of the dynamic behavior and heat transfer characteristics of water droplets impinging upon a heated surface, Int. J. Heat Mass Transfer 13 (1970) 369-381.

[12] F.K. McGinnis, III, J.P. Holman, Individual droplet heat-transfer rates for splattering on hot surfaces, Int. J. Heat Mass Transfer 12 (1969) 95-108.

[13] T.Y. Xiong, M.C. Yuen. Evaporation of a liquid droplet on a hot plate, Int. J. Heat Mass Transfer 34 (1991) 1881-1894.

[14] K.J. Baumeister, T.D. Hamil and G.J. Schoessow, A generalized correlation of vaporization times of drops in film boiling on a flat plate, Third Int. Heat Transfer Conf. 4 (1966) 66-73.

[15] B.S. Gottfried, C.J. Lee, K.J. Bell, The Leidenfrost Phenomenon: film boiling of liquid droplets on a flat plate, Int. J. Heat Mass Transfer 9 (1966) 1167-1187.

[16] M. Ciofalo, I. DiPiazza, V. Brucato, Investigation of the cooling of hot walls by liquid water sprays, Int. J. Heat Mass Transfer 42 (1999) 1157-1175.

[17] J.H. Kim, S.M. You, S.U.S Choi, Evaporative spray cooling of plain and microporous coated surfaces, Int. J. Heat Mass Transfer 47 (2004) 3307-3315.